

Fabrication of Titanium Aluminide Matrix Composites by Laser Engineered Net Shaping

Weiping Liu and John DuPont

Department of Materials Science and Engineering, Lehigh University, Bethlehem, PA 18015

Abstract

TiAl-based titanium aluminide alloys and their composites reinforced with ceramic particles are considered to be important candidate materials for high temperature structural applications. Laser Engineered Net Shaping (LENS) is a layered manufacturing process, which involves laser processing fine powders into three-dimensional components directly from a CAD design. In this work, the LENS process has been employed to fabricate carbide particle reinforced titanium aluminide matrix composites using TiC and gas-atomized Ti-48Al-2Cr-2Nb powders as the feedstock materials. The composites deposited by the LENS process exhibited a susceptibility to solid-state cracking due to the generated high thermal stresses. The microstructures of the laser-deposited monolithic and composite titanium aluminide materials were characterized using light optical microscopy and XRD techniques. Effects of the LENS processing parameters on the cracking susceptibility and microstructure were studied. Crack-free deposits can be fabricated by preheating the substrate to 450~500°C during LENS processing. The fabricated composite deposits exhibit a hardness of more than twice the value of the Ti-6Al-4V alloy.

Keywords: LENS processing; Titanium aluminides; Composites; Direct laser fabrication

1. Introduction

Titanium aluminide alloys based on TiAl and their composites reinforced with ceramic particles have been considered and are being developed for high temperature applications in the automotive, aerospace and power generation industries [1]. The TiAl-based alloys have several advantages over the conventional titanium alloys, such as higher elasticity modulus, lower density, better mechanical properties at elevated temperatures and higher oxidation resistance due to the formation of a surface passivated alumina layer [2]. The intermetallic-matrix composites (IMCs) reinforced with ceramic particles generally possess even higher specific strength, specific stiffness, increased creep strength, improved toughness and high temperature strength retention. Discontinuously reinforced intermetallic-matrix composites have been produced by a variety of techniques, most of which rely on a powder processing route including mechanical alloying and combustion reaction synthesis or reactive sintering technique, cryomilling, reactive hot isostatic pressing and XD synthesis [3]. Despite a number of advantages, fabrication of IMCs by powder metallurgical processing generally requires the use of dies for pressure-aided densification, which limits its applications.

Laser Engineered Net Shaping (LENS) is a solid freeform fabrication (SFF) process, which involves laser processing fine powders into fully-dense three-dimensional components directly from a CAD design. A variety of metals and alloys have been deposited by LENS processing, such as H13 steel, 316 stainless steel, nickel-base superalloys and titanium alloys [4-7]. However, little work has been done on processing titanium aluminide intermetallics by LENS although a few papers were published on microstructural characterization of laser-deposited TiAl alloys

[8-9]. So far, no effort has been made to fabricate aluminide intermetallic matrix composites by LENS.

In this work, a feasibility study has been conducted to fabricate carbide particle reinforced titanium aluminide matrix composites by LENS processing using TiC and gas-atomized Ti-48Al-2Cr-2Nb powders as the feedstock materials. Two types of applications are expected for the LENS processing of ceramic particle reinforced titanium aluminide matrix composites. One is the fabrication of deposits on a titanium substrate alloy in order to improve its resistance to high temperature and/or other surface properties such as wear resistance. The other is the rapid production of a three-dimensional component of the intermetallic matrix composite.

2. Experimental Procedure

The materials used in this investigation were gas-atomized pre-alloyed Ti-48Al-2Cr-2Nb (in at.%) powder obtained from Crucible Research, and TiC powder (purity 99.9%) from Atlantic Equipment Engineers. All the powders have a mesh size of -100/+325 (particle sizes between 45 and 150 μm). A hot-rolled Ti-6Al-4V plate of 3.175 mm in thickness was used as the substrate material, which had a composition of 6.1 Al, 4.3 V (in wt.%) and was obtained from Trans-World Alloys. It is a typical ($\alpha+\beta$) Ti alloy of wide industrial applications. The microstructure of the Ti-6Al-4V substrate is composed of equiaxed and elongated α and intergranular β phases. The substrate was ground with 320 grit SiC paper, and then degreased using acetone and ethanol before deposition.

In the present work, an Optomec LENS 750 machine was used to deposit the samples, which has a size of 12.7 mm \times 12.7 mm \times 8 layers. The LENS machine consists of a 750 W Nd:YAG laser, a 4-nozzle coaxial powder feed system, a controlled environment glove-box and a motion control system [10]. For fabrication of the composite deposits, 10 and 20 vol% TiC powder respectively, were added to the Ti-48Al-2Cr-2Nb powder and mixed thoroughly before being loaded into the powder feeder. Since TiC has a similar density (4.9 g/cm³) to that of Ti-48Al-2Cr-2Nb (4.5 g/cm³), homogeneous mixing can be achieved. Monolithic Ti-48Al-2Cr-2Nb deposits were also produced for comparison. Different laser powers (from 170 to 340 W) and traverse speeds (from 4.2 to 16.9 mm/s) were used in the experiments. The powder feed rate varied from 2.4 to 3.5 g/min according to the traverse speed. The layer thickness, hatch spacing, and stand-off distance were set at 0.254 mm, 0.381 mm and 152.4 mm respectively. The oxygen level in the glove box was kept below 6 ppm during processing. Light optical microscopy, electronic probe micro-analysis (EPMA) and XRD were used for microstructure and phase analysis. The surfaces of cracks were examined with a JEOL 6300 SEM. Microhardness measurements were conducted on selected specimens using a Vickers indenter under a 300 gram load.

3. Results and Discussion

3.1 Microstructure and phase analysis

Fig. 1 shows the microstructure of a Ti-48Al-2Cr-2Nb deposit processed with a laser power 300 W and 6.4 mm/s traverse speed. The microstructure of as-deposited monolithic Ti-48Al-2Cr-2Nb consists of massively transformed γ phase (dark contrast) and a small amount of α_2 phase (light contrast). The α_2 phase was mostly observed in the first layer adjacent to the

substrate (as shown in Fig. 1a) and at the bottom of a layer in a vertical cross-section or at the inter-track region in a horizontal cross-section. This is because the cooling rate is much higher at these regions under the heat conduction conditions during processing, such that the massive transformation to γ phase is incomplete and the high-temperature α phase is ordered to α_2 phase. As is recently known [11-12], the $\alpha \rightarrow \gamma$ massive transformation occurs when the cooling rate is high enough for the growth of lamellae or Widmanstatten laths to be suppressed, but not so high

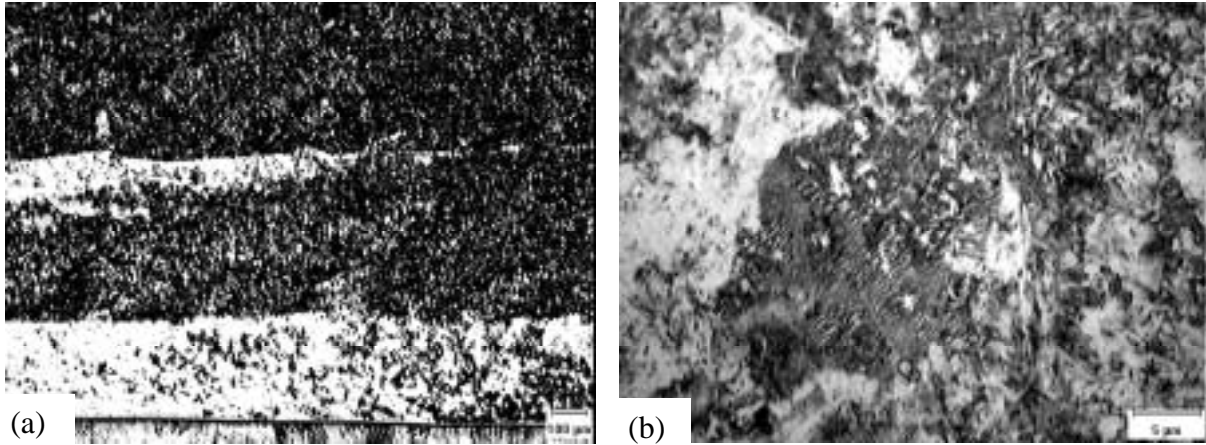


Fig. 1 Microstructure of as-deposited monolithic Ti-48Al-2Cr-2Nb alloy: (a) near the substrate; (b) massively transformed γ phase.

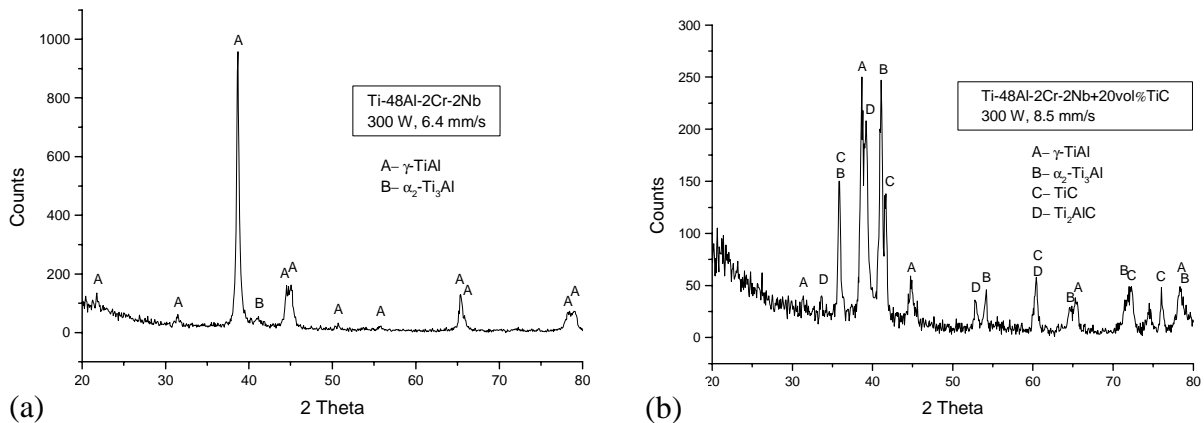


Fig. 2 X-ray diffraction patterns of LENS deposits of (a) Ti-48Al-2Cr-2Nb and (b) Ti-48Al-2Cr-2Nb+20 vol% TiC.

that the $\alpha \rightarrow \alpha_2$ transformation (ordering reaction) takes place. The latter transformation should be avoided or kept at a minimum through a proper choice of processing parameters since the Al-supersaturated α_2 (Ti_3Al) phase is extremely brittle. As shown in Fig. 2(a), the result of X-ray diffraction conducted on the surface perpendicular to the build direction confirms that the sample contains γ and α_2 phases, and the intensity of diffractive peaks for α_2 is very weak due to a small volume fraction.

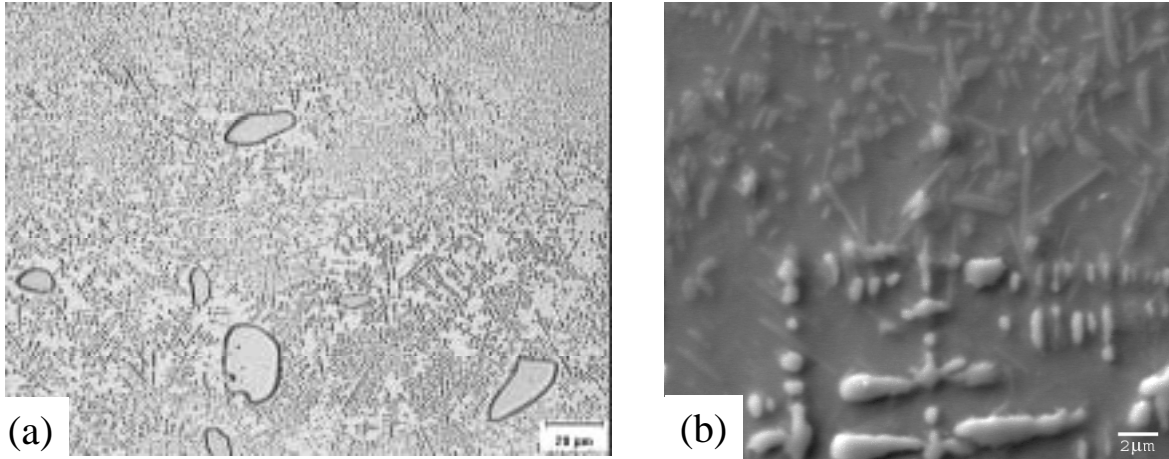


Fig. 3 Microstructure of Ti-48Al-2Cr-2Nb+20v%TiC composite deposit (as-polished) processed with a 300 W laser power and 8.5 mm/s traverse speed: (a) light micrograph; (b) SEM micrograph.

The micrograph in Fig. 3 shows that the microstructure of Ti-48Al-2Cr-2Nb+20v%TiC deposit fabricated using a 300 W laser power and 8.5 mm/s traverse speed consists of unmelted TiC particles, dendritic and needle-like phases (Fig. 3b at higher magnification) distributed in the titanium-aluminide matrix. The XRD result (Fig. 2b) indicates that TiC and Ti₂AlC carbides are present in the sample in addition to γ and α_2 matrix phases. Compared with Fig. 2a, the relative intensity of diffractive peaks for α_2 in the composite deposit is significantly enhanced, indicating an increase in the volume fraction. The electronic probe micro-analysis conducted on the sample revealed that the dendritic phase is mainly composed of Ti and C (about 17.7 wt% carbon) with a small amount of Al and Nb. Thus, the dendritic phase is the primary TiC formed from the melt upon cooling.

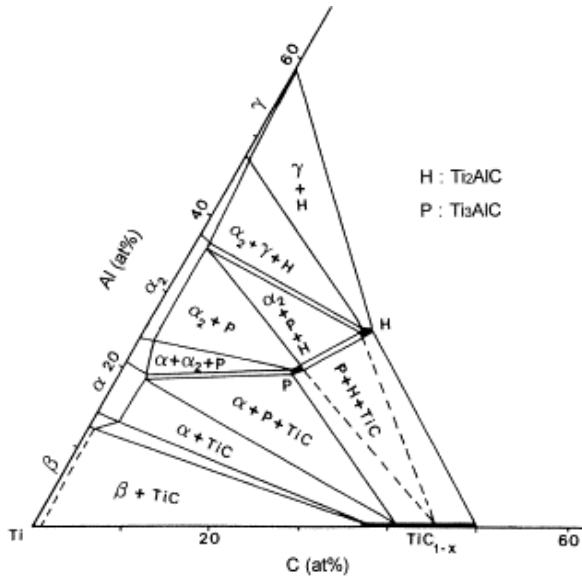


Fig. 4 A partial isothermal section of the Ti-Al-C ternary system at 1050°C [14].

Under laser beam irradiation, the substrate and powders absorb energy from the beam and form a melt pool. It is known that the laser absorption coefficient (α) of a material is a function of temperature, its electrical resistivity and the laser's wavelength [13], as given by:

$$\alpha(T) = 0.365 \left\{ \rho_{20} [1 + \rho(T-293)] / \lambda \right\}^{0.5} - 0.0667 \left\{ \rho_{20} [1 + \rho(T-293)] / \lambda \right\} + 0.006 \left\{ \rho_{20} [1 + \rho(T-293)] / \lambda \right\}^{1.5}$$

where, ρ and ρ_{20} are the material's electric resistivity (in Ωcm) at temperature T and 20°C respectively, λ is the incident laser's wavelength, and T is temperature (in K). The TiC powder

particles have a much larger value of electric resistivity than the titanium aluminide particles, and therefore a higher absorption coefficient. In addition, the heat conductivity of TiC is lower. Consequently, in spite of its high melting point (3067°C) partial melting of the TiC powder particles occurred in the melt pool. As indicated in Fig.3, the particle size of unmelted TiC is much smaller than the starting particle size (45 to 150 μm). It was also found that the amount of melted TiC is dependent on the processing parameters used. The amount of melted TiC increased with the increasing laser incident energy or heat input (incident laser power over traverse speed). The melted TiC mixing with the molten Ti-48Al-2Cr-2Nb formed a Ti-Al-C-Cr-Nb liquid in the melt pool. The amount of melted TiC was estimated to be approximately 50% of the total amount through image analysis for the sample shown in Fig. 3(a). The composition of the liquid formed in the melt pool was then calculated to be Ti-40.9Al-6.7C-1.8Cr-1.8Nb. According to a partial isothermal section of the Ti-Al-C ternary system at 1050°C [14], the microstructure in equilibrium for this composition consists of H (Ti₂AlC), γ and α₂ phases without the presence of TiC phase, as shown in Fig. 4. The discrepancy from the observed microstructure can be

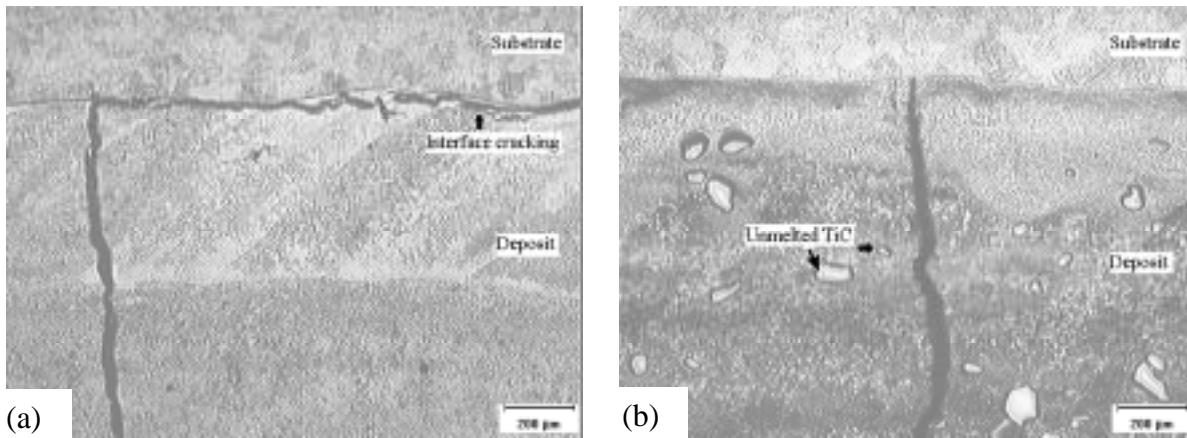


Fig. 5 Cracks observed in (a) Ti-48Al-2Cr-2Nb (300 W, 8.5 mm/s) and (b) Ti-48Al-2Cr-2Nb+20v%TiC (250 W, 6.4 mm/s) deposits.

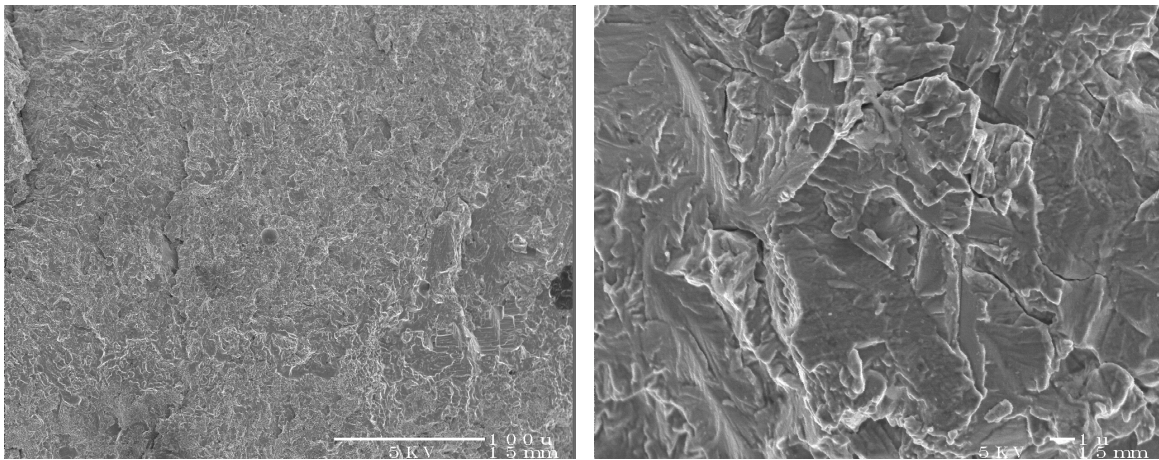


Fig. 6 SEM fractographs at different magnifications of crack surfaces observed in a Ti-48Al-2Cr-2Nb deposit (300W, 10.6 mm/s).

explained from the solidification path under rapid cooling conditions. According to a partial TiAl-TiC section of Ti-Al-C system proposed by Zakharov et al [15], at a carbon content higher than about 2 at.% primary TiC_{1-x} solidifies first from the melt at high temperatures ($>2200^{\circ}C$), then a peritectic reaction $TiC_{1-x} + L \rightarrow Ti_2AlC$ takes place at about $2200^{\circ}C$. Below this temperature, the Ti_2AlC ternary carbide can also precipitate from the liquid due to a decrease in carbon content of the liquid composition. Another peritectic reaction $L + Ti_2AlC \rightarrow TiAl$ can occur later. According to Cam et al [14], a reaction $L + \beta \rightarrow \alpha + Ti_2AlC$ may take place at the final stage. On the basis of the available information, the phase transformation process may be described as $L \rightarrow TiC+L \rightarrow TiC+Ti_2AlC+L \rightarrow TiC+Ti_2AlC+\beta+L \rightarrow TiC+Ti_2AlC+\alpha \rightarrow TiC+Ti_2AlC+\gamma(TiAl)+\alpha_2(Ti_3Al)$. The observed increase of α_2 volume fraction in the composites from the XRD results can be attributed to the fact that carbon atoms in solid solution promote the stability of the high-temperature α phase [16]. It can also be found from the Ti-Al-C phase diagram in Fig. 4 that the solubility of carbon in α_2 phase is much higher than that in γ phase.

3.2 Cracking problem and its prevention

The principal problem initially encountered in depositing both the monolithic and composite titanium aluminides by LENS is the occurrence of cracking in the deposits. In most cases, the observed cracks originated from the edge or surface of the samples with the crack plane being perpendicular to the substrate (Fig. 5). But cracking was sometimes also seen to occur at the interface between the deposit and the substrate, as shown in Fig. 5a. Fig. 6 shows the representative SEM fractographs of the crack surfaces in Ti-48Al-2Cr-2Nb deposits. As can be seen, fracture occurred principally by transgranular cleavage, which is typical of failure in titanium

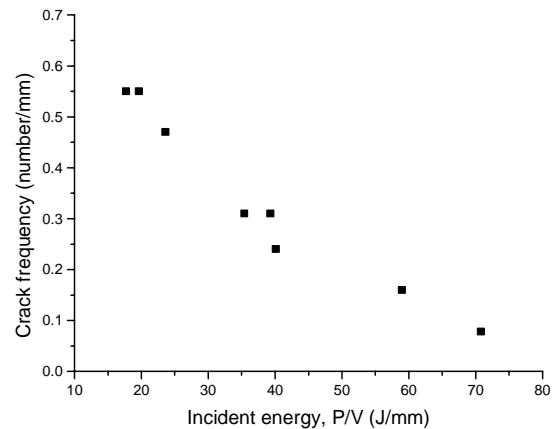


Fig. 7 Dependence of cracking frequency on the incident laser energy for the composite deposits.

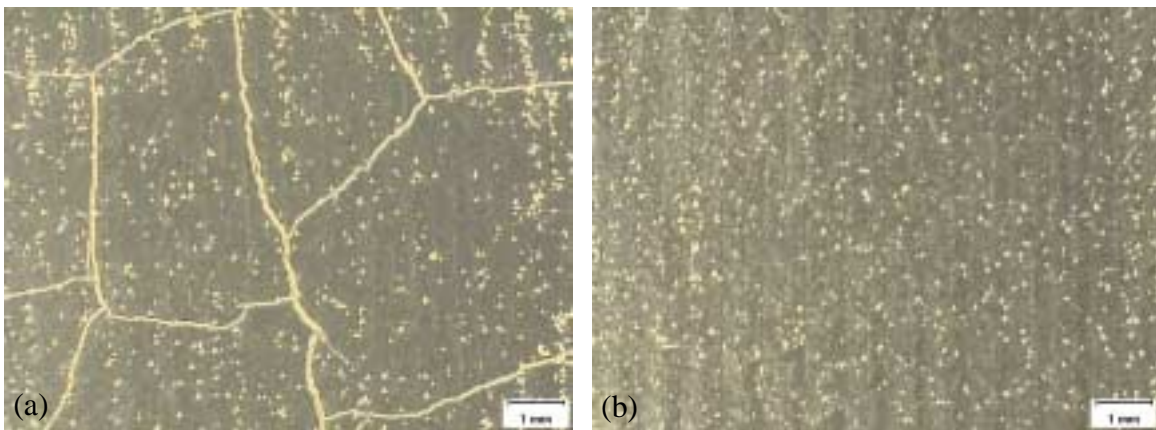


Fig. 8 Effectiveness of preventing cracking in Ti-48Al-2Cr-2Nb+TiC composite deposits by heating the substrate during processing: (a) without preheating; (b) heating to $450^{\circ}C$.

aluminide intermetallics. The cracking is therefore a type of solid-state cracking. It was also found that the number of cracks (crack frequency) in the vertical cross-section of the cracked deposits varied according to the processing parameters used (the incident laser power (P) and traverse speed (V)). As shown in Fig. 7, crack frequency decreased as the incident energy (P/V) of laser beam was increased. It is known from the welding research that the cooling rate in the laser deposition process is mainly dependent upon the heat input (P/V) for a given material. For a point heat source traveling in a semi-infinite medium, according to the Rosenthal's 3-D solution [17], the cooling rate is inversely proportional to the laser heat input (P/V) as given by:

$$\partial T/\partial t \propto k(T-T_0)^2/(P/V)$$

where k is the thermal conductivity of the material, T₀ is the substrate temperature. The reduced cracking propensity at higher heat inputs is ascribed to the resulting lower cooling rates. It is believed that cracking was caused by a high level of thermally-induced stresses exceeding the material's fracture strength in a temperature range where ductility of the material is minimal, as also indicated by Patterson et al [18] in their weldability study of a titanium aluminide alloy. A higher cooling rate increases the thermally-induced stresses, leading to an increase in cracking susceptibility. As the ductility of the intermetallic alloys and composites is relatively lower than that of steels and conventional alloys, these materials are more susceptible to cracking during LENS processing.

Experiments indicated that it is difficult to eliminate cracking in the deposits only by regulating the processing parameters although cracking can be mitigated in this way. A hot plate was used to preheat the substrate to 450~500°C during LENS processing for preventing the solid-state cracking. The results show that crack-free deposits can be produced using a general combination of processing

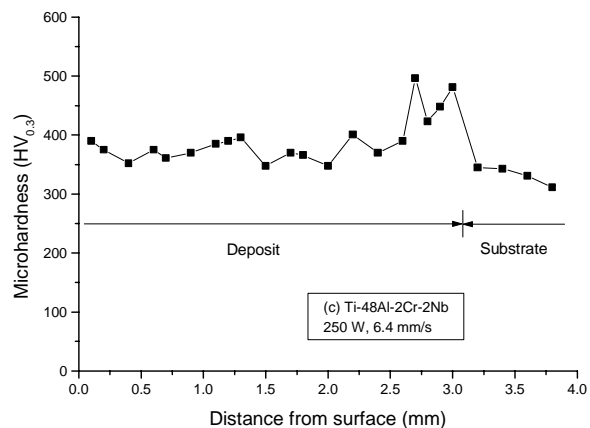
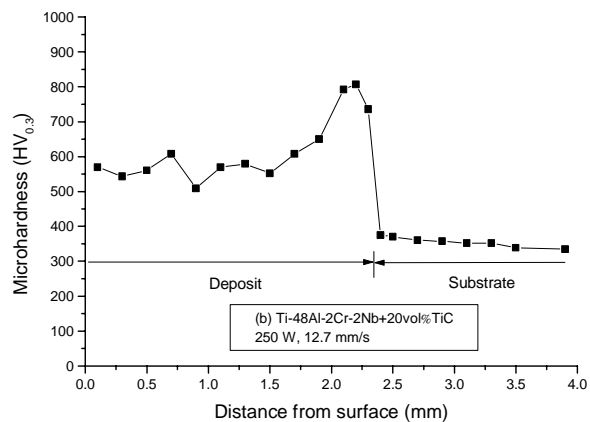
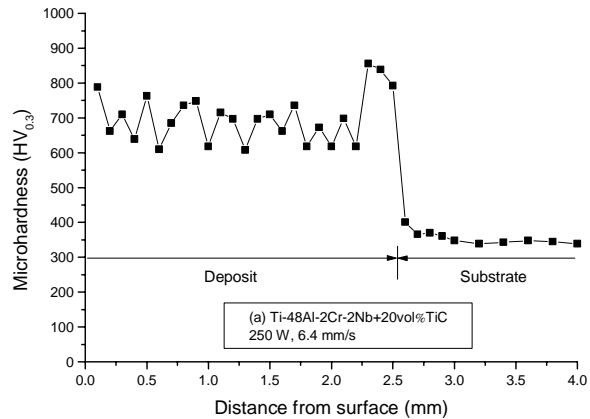


Fig. 9 Microhardness distributions: (a) and (b) the composite deposits; (c) monolithic titanium aluminide deposits.

parameters (for 300 W incident laser power, traverse speed less than 12.7 mm/s) if substrate heating is conducted. Fig. 8 shows photographs of as-polished surfaces of the aluminide composites deposited without and with substrate heating during processing using the same parameters, respectively. It is therefore a very effective method for eliminating cracks in the LENS deposits.

3.3 Microhardness

The microhardness ($HV_{0.3}$) was measured from the deposit surface down to the substrate. Fig. 9 (a) and (b) show the hardness distributions for the composite deposits processed at different traverse speeds, while Fig. 9(c) is the result for a monolithic titanium aluminide deposit for comparison. The measured microhardness values for the composite are the overall bulk hardness without the inclusion of unmelted TiC particles (i.e. the microhardness data are not used when the indenter hit unmelted TiC particles). The microhardness of the unmelted TiC particle was measured to be 2240~2390 Vickers hardness number (VHN). For the Ti-48Al-2Cr-2Nb+20v%TiC composite deposits, the one processed with a slower speed is harder with an average hardness of 700 VHN, which is approximately 2.2 times that of the substrate (320 VHN). This is because the deposit contains more re-solidified TiC and Ti_2AlC carbides resulting from a larger amount of melted TiC when a slower traverse speed is used at a same laser power. The large scatter of the measured hardness in the deposit was due to the inhomogeneous distributions of the dendritic and needle-like carbides together with γ and α_2 matrix phases of different hardness. The monolithic titanium aluminide deposit has an average hardness value of 380 VHN, which is similar to that obtained by the conventional processes. It is noted that in all cases the hardness in the layer adjacent to the substrate is the highest. Based on microstructural analysis, it is found that the volume fraction of α_2 phase is higher in the first layer as a result of the dilution of the substrate combined with a higher cooling rate. The heat-affected zone (HAZ) has a slightly higher hardness than that of the substrate as the HAZ has an acicular martensite structure (the supersaturated α' -phase). The high hardness of the composite deposits is expected to exhibit an excellent wear resistance. In addition, through compositional and processing optimization, the carbide reinforced γ -TiAl matrix composites are also expected to possess improved strength and fracture toughness. Further work is needed in these aspects.

4. Conclusions

A feasibility study has been conducted to fabricate carbide-particle-reinforced TiAl matrix composites using TiC and Ti-48Al-2Cr-2Nb powders as the feedstock materials by LENS processing. Both the monolithic and composite titanium aluminide deposits exhibited a susceptibility to solid-state cracking due to the high thermal stresses generated from the LENS processing. Crack-free deposits can be fabricated by preheating the substrate during LENS processing. The microstructure of fabricated composite deposits consists of unmelted TiC particles with resolidified TiC and Ti_2AlC carbides distributed in γ and α_2 matrix phases. The microstructure of monolithic Ti-48Al-2Cr-2Nb deposits is composed of massively transformed γ phase and a small amount of α_2 phase. The fabricated composite deposits exhibit a hardness of more than twice the value of the Ti-6Al-4V alloy.

Acknowledgements

The authors gratefully acknowledge support of this work by the National Science Foundation through a PECASE Award, Grant No. DMI 9983968, made through the Division of Manufacturing and Industrial Innovation of NSF.

References

- [1] Y.-W. Kim, D.M. Dimiduk, M.H. Loretto (eds), *Gamma Titanium Aluminide 1999*, TMS, Warrendale, PA, 1999.
- [2] S. Djanarthany, J.C. Viala, and J. Bouix, *Materials Chemistry and Physics* 72 (2001) 301-319.
- [3] C.M. Ward-Close, R. Minor, and P.J. Doorbar, *Intermetallics* 4 (1996) 217-229.
- [4] G.K. Lewis, E. Schlienger, *Materials and Design* 21 (2000) 417-423.
- [5] P.A. Kobryn, E.H. Moore and S.L. Semiatin, *Scripta Mater.* 43 (2000) 299-305.
- [6] M. Griffith, L.D. Harwell, J.A. Romero, E. Schlienger, C.L. Atwood, J.E. Smugeresky, in: *Proceedings of the Solid Freeform Fabrication Symposium*. Austin, TX, August 1997: 387.
- [7] W. Hofmeister, M. Griffith, M. Ensz, and J. Smugeresky, *JOM* 53 (9) (2001) 30-34.
- [8] X.D. Zhang, C. Brice, D.W. Mahaffey, H. Zhang, K. Schwendner, D.J. Evans and H.L. Fraser, *Sripta Mater.* 44 (2001) 2419-2424.
- [9] D. Srivastava, I.T.H. Chang, and M.H. Loretto, *Intermetallics* 9 (2001) 1003-1013.
- [10] LENSTM 750 user's manual, Optomec, NM.
- [11] A. Denquin and S. Naka, *Acta Mater.* 44 (1996), 353-365.
- [12] Q. Xia, J.N. Wang, J. Yang, and Y. Wang, *Intermetallics* 9 (2001) 361-367.
- [13] W.W. Duley, *CO₂ Lasers: Effects and Applications*, Academic Press, NY, 1976.
- [14] G. Cam, H. Flower, D. West, *Materials Science and Technology* 7 (1991), 505-511.
- [15] P. Villars, A. Prince, and H. Okamoto, *Handbook of Ternary Alloy Phase Diagrams (Vol.3)*, ASM International, Materials Park, OH, 1995: 2908.
- [16] F. Perdrix, M. Trichet, J. Bonnentien, M. Cornet, and J. Bigot, *Intemetallics* 9 (2001) 807-815.
- [17] S. Kou, *Welding Metallurgy*, John Wiley & Sons, Inc. 1987.
- [18] R.A. Patterson, P.L. Martin, B.K. Damkroger, and L. Christodoulou, *Welding Journal*, 69 (1) (1990), 39s-44s.